JACS
JOURNAL OF THE AMERICAN CHEMICAL SOCIETY
Communication
pubs.acs.org/JACS

Nanostar and Nanonetwork Crystals Fabricated by in Situ Nanoparticlization of Fully Conjugated Polythiophene Diblock Copolymers

In-Hwan Lee,[†] Pitchamuthu Amaladass,[†] Ki-Young Yoon,[†] Suyong Shin,[†] Yong-Jae Kim,[‡] Inhye Kim,[‡] Eunji Lee,[‡] and Tae-Lim Choi*[,†]

[†]Department of Chemistry, Seoul National University, Seoul, 151-747, Korea

[‡]Graduate School of Analytical Science and Technology, Chungnam National University, Daejeon, 305-764, Korea

Supporting Information

ABSTRACT: Nanostar and nanonetwork crystals were prepared from fully conjugated poly(3-(2-ethylhexyl)-thiophene)-*block*-polythiophene (P3EHT-*b*-PT) via a simple INCP process. The structural conformation of the nanocrystals was investigated in detail, revealing that with an increase in the block length of PT, the morphology of the nanocrystals changed from nanospheres to nanorods, nanostars, and to nanonetworks.

Self-assembly of block copolymers in solution has produced intriguing nanostructures such as worm-like[1] and multi-compartment[2] micelles and vesicles.[3] Self-assembly of conjugated polymers is particularly intriguing because these polymers may yield well-defined, semiconducting nano-objects for prospective use as optoelectronic materials with tunable bandgaps.[4] For example, self-assembly of rod−coil block copolymers based on polythiophene derivatives afforded ordered nanostructures such as spherical[5] and fiber-like[6] micelles, and self-assembly of fully conjugated rod−rod polythiophene diblock copolymers produced ordered nanostructures such as nanowires,[7] nanorings,[7b] helical nanowires,[8] and vesicles.[3b] However, the self-assembly processes generally required postsynthetic treatments such as addition of selective solvents and additives, because the synthesis of the block copolymers itself did not provide sufficient driving force to assemble the polymers into the nanostructures. In addition, the generated nanostructures are generally fragile toward the changes in the external conditions such as temperature, solvents, and mechanical stress. Recently, our group developed a simple one-pot direct process for spontaneous and irreversible formation of highly stable 0-(0D) and one-dimensional (1D) nanostructures by in situ nanoparticlization of conjugated polymers (INCP) using soluble polymers as the first block and insoluble conjugated polymers as the second block.[9] For example, diblock copolymers (PN-*b*-PA) comprised of soluble polynorbornene and completely insoluble polyacetylene were synthesized by ring-opening metathesis polymerization (ROMP); the resulting PN-*b*-PA spontaneously formed highly stable nanospheres or unique nanocaterpillars depending on the block ratio.[9a] Strong $\pi-\pi$ interaction on the PA block resulting in solvophobic interaction provided a strong driving force for this in situ nanoparticlization. Although the previous examples of INCP provided intriguing nanostructures from very simple diblock copolymers, the application of these nanostructures to electronic materials was limited by the insulating PN shells on the nanostructures that may hinder the efficient charge transport. Furthermore, PA (having a shallow highest occupied molecular orbital (HOMO) level) is generally susceptible to oxidation in air, thus compromising the long-term stability of the nanoparticles under ambient conditions. Consequently, to enhance the conductivity and stability of the nanostructures in air, the design of the block copolymer must be modified to incorporate both soluble and insoluble conjugated polymers such as polythiophene derivatives. Moreover, these preorganized nanostructures via INCP, comprising fully conjugated polymers may have many potential advantages over the conventional conjugated polymers in terms of electronic performance, facilitating the charge carrier transport through well-defined pathways provided by well-ordered crystalline domains.[10] Furthermore, because the stable nanostructures have already been formed, additional post-treatment processes such as thermal or solvent vapor annealing would be unnecessary.[10]

Branched nanostructures such as tetrapods have attracted great attention because of their unique structures and potential optoelectronic applicability.[2b−d,6d,11,12] However, the majority of branched nanostructures have been derived from inorganic materials;[11] only a handful of polymer-based examples have been reported.[2b−d,6d,12] Branched nanostructures containing conjugated polymers are particularly rarely reported.[6d,12a] Herein, we report the formation of unique branched semiconducting nanostructures such as nanostars and nanonetworks via INCP of diblock copolymers containing a block of soluble poly(3-(2-ethylhexyl)thiophene) as the first block and insoluble polythiophene (P3EHT-*b*-PT) as the second block. These nanostar and nanonetwork are kinetically trapped nanostructures that are spontaneously and irreversibly formed during polymerization but are highly stable toward external stimuli such as heat and mechanical stress.

Synthesis of fully conjugated polythiophene diblock copolymers was achieved via the quasi-living Grignard metathesis (GRIM) method.[13] 2,5-Dibromo-3-(2-ethylhexyl)thiophene (**1**) and 2,5-dibromothiophene (**2**) were selected as monomers for INCP, because P3EHT is highly soluble (solvophilic) in the

Received: September 5, 2013
Published: November 13, 2013

dx.doi.org/10.1021/ja409206p | *J. Am. Chem. Soc.* 2013, 135, 17695−17698

reaction solvent, i.e., tetrahydrofuran (THF), and PT is totally insoluble (solvophobic) in any organic solvent because of the strong intermolecular interactions (Table 1). Using a catalyst loading of 1 mol % of (1,3-bis(diphenylphosphino)propane) dichloronickel(II) ($Ni(dppp)Cl_2$) with respect to monomer **1**, three different samples with various feed ratios of **1**:**2**, such as 100:33, 100:67, and 100:100, were prepared (Table 1). The number average molecular weight (M_n) of the first block, P3EHT, was determined by THF size exclusion chromatography (SEC), and the values of M_n and polydispersity index (PDI) of the P3EHT component for all three samples were ~10 kg/mol and 1.2, respectively, suggesting that GRIM was well-controlled (Table 1, entries 1−3). The degree of polymerization (DP) of the second PT block was estimated using gas chromatography-mass spectrometry (GC-MS), and the DP of PT increased linearly with an increase in the equivalent of **2** (Table 1, entries 1−3). All three nanoparticles from P3EHT-*b*-PT were soluble and stable in common organic solvents such as THF, chloroform, toluene, and chlorobenzene.

The first indication of successful INCP using P3EHT-*b*-PT was obtained from the NMR analysis. Both the ^1H and ^{13}C NMR spectra of the samples in $CDCl_3$ were identical to those of the P3EHT homopolymer (Figure S1). This observation is typical for core−shell-type supramolecules formed via INCP, implying that the stacked PT block formed the core that was not solvated by $CDCl_3$; thus, the signal for PT was not detected.[9]

The second indication of successful INCP was the significant color change and UV−vis analysis provided insightful information on the changes in the polymer nanostructures. When **2** was added to the P3EHT solution with living chain ends, the initial orange color first changed to red and then to dark purple within 10 min, and the UV−vis spectra revealed the following changes: the absorbance maximum (λ_{max}) of the initial homopolymer of P3EHT in toluene was observed at 437 nm, and the onset point at 525 nm corresponded to a bandgap (E_g) of 2.4 eV (Figure 1). In comparison, the spectra of the block copolymer in toluene were significantly red-shifted with λ_{max} values of 455, 469, and 544 nm (increased by 18, 32, and 107 nm, respectively) for $P3EHT_{100}$-*b*-PT_{33}, $P3EHT_{100}$-*b*-PT_{67}, and $P3EHT_{100}$-*b*-PT_{100}, respectively. The onset points of the stated P3EHT-*b*-PT also increased to 621−626 nm (E_g = 2.0 eV) (Figure 1). Moreover, two new distinct vibronic peaks for P3EHT-*b*-PTs appeared at 544 and 590 nm, even in the solution state (Figure 1). Overall, the extent of the red-shifts of λ_{max} and the onset points and the intensity of the new vibronic peaks increased in accord with the DP of PT. These observations suggest that the solvophobic second PT block formed a well-ordered core even in solution. Similar to the solution cases, the UV−vis spectra of P3EHT-*b*-PT in the film state were characterized by an increase in the intensities of the vibronic peaks with increasing DP of PT (Figure S2a). The UV−vis spectra of the thermally annealed samples in the film state showed that even up to 150 °C, there was no significant change in the UV−vis spectra for each film (Figure S2c−e)). In particular, the UV−vis spectra of $P3EHT_{100}$-*b*-PT_{100} in the solution and film states were almost superimposable, suggesting that no additional improvement in the ordering was derived from annealing of the film relative to the solution state (Figure S2e). In short, the morphologies of the cores of the nanostructures formed from P3EHT-*b*-PT in solution and film were very similar; in particular, the packing of $P3EHT_{100}$-*b*-PT_{100} in solution was as well-ordered as that in the film state.

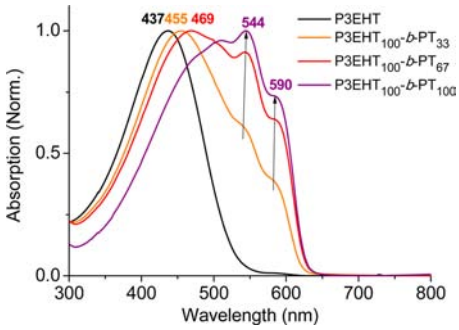

Figure 1. UV−vis spectra of nanostructures from P3EHT-*b*-PT in toluene.

Detailed information on the crystallinity of the supramolecules was obtained from powder X-ray diffraction (PXRD) and differential scanning calorimetry (DSC) analyses. PXRD showed two distinct peaks for all of the P3EHT-*b*-PT samples (Figure S3). The first peak corresponded to the (100) reflection of P3EHT with a *d*-spacing of 1.46 nm, and the second peak with a *d*-spacing of 0.45 nm was ascribed to the (010) and (110) reflections of P3EHT and PT, respectively (Figure S3).[14,15] The peak intensity corresponding to the *d*-spacing of 0.45 nm increased as the DP of PT increased, implying that the (110) reflection from PT was dominant for the second peak (Figure S3). The increase in the intensity of the (110) peak from the PXRD pattern and the vibronic peaks in the solution UV−vis spectra of P3EHT-*b*-PT with a higher DP of PT confirmed the enhanced interaction and crystallinity of the PT core (Figures 1 and S3). The melting temperature (T_m) of P3EHT-*b*-PT was ~60 °C, based on DSC, which corresponded to the T_m of the first block, P3EHT (Figure S4). The T_m of P3EHT-*b*-PT was relatively lower than that of the parent P3EHT (70−90 °C),[16] suggesting lower crystallinity of the former because of the loose packing of the first block in the restricted geometry of the core−shell structure. In the case of $P3EHT_{100}$-*b*-PT_{100}, there was an additional T_m at 125 °C, whose origin is unclear at present. In comparison, no T_m was observed for the PT homopolymer in the range 20−350 °C, and the T_m associated with PT was not observed for any of the three P3EHT-*b*-PT (Figure S4).

To obtain size and structural information of the supramolecules, we carried out dynamic light scattering (DLS), atomic force microscopy (AFM), and transmission electron microscopy (TEM) analyses. The DLS measurement confirmed that the hydrodynamic diameter (D_h) of the supramolecules in toluene gradually increased from 90 to 673 nm with an increase in the DP of PT (Figure 2). The AFM imaging of $P3EHT_{100}$-*b*-PT_{33} on

Table 1. Synthesis of P3EHT-*b*-PT

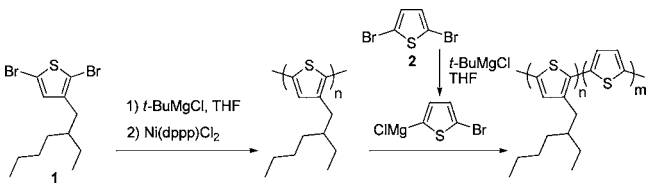

entry	[Ni cat.]:[**1**]:[**2**]	M_n (PDI) of P3EHT[a]	DP of PT[b]	yield
1	1:100:33	9.3k (1.25)	27	40%
2	1:100:67	9.9k (1.23)	58	44%
3	1:100:100	12.4k (1.23)	80	50%

[a]Determined by THF SEC calibrated using PS standards. M_n is given in g/mol. [b]Estimated by GC-MS.

dx.doi.org/10.1021/ja409206p | J. Am. Chem. Soc. 2013, 135, 17695−17698

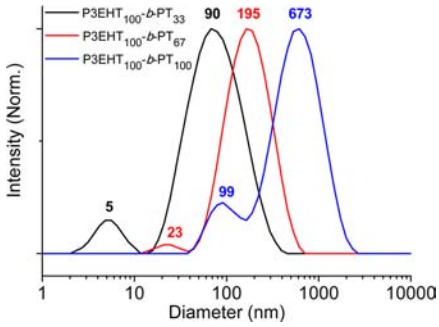

Figure 2. DLS profiles of P3EHT-*b*-PT nanocrystals in toluene.

highly ordered pyrolytic graphite (HOPG) revealed a mixture of nanospheres and nanorods (40−100 nm long) with 1−3 nm in height (Figures 3a and S6a). The bimodal trace from the DLS profile showing average D_h values of 90 nm (major) and 5 nm (minor) may correspond to the nanorods and nanospheres, respectively (Figure 2). The AFM images of P3EHT$_{100}$-*b*-PT$_{67}$ mostly showed the formation of a new star-shaped nanostructure (nanostar), exhibiting unique branching (Figures 3b and S6b). The height of the nanostar on HOPG was 3−6 nm and much

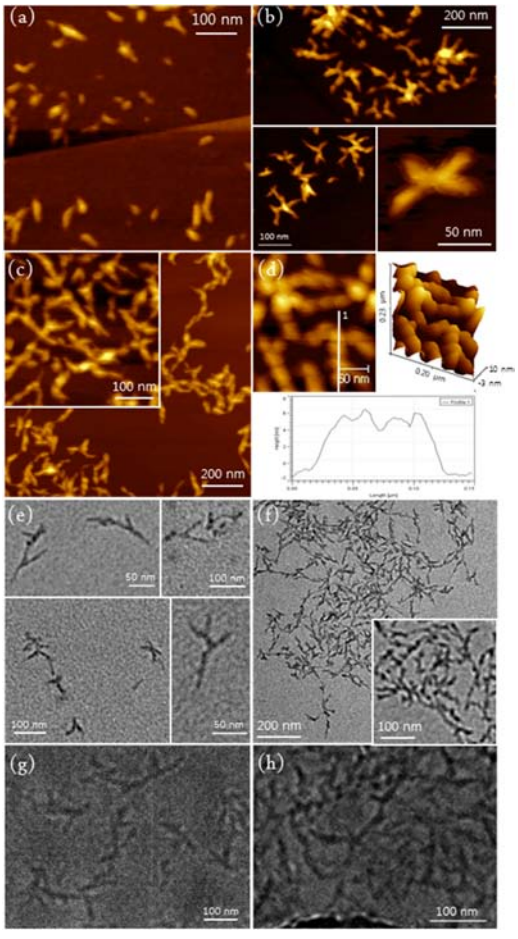

Figure 3. AFM, TEM, and cryo-TEM images of nanostructures from various P3EHT-*b*-PT. AFM images of nanostructures from (a) P3EHT$_{100}$-*b*-PT$_{33}$, (b) P3EHT$_{100}$-*b*-PT$_{67}$, and (c) P3EHT$_{100}$-*b*-PT$_{100}$. (d) Side-view and cross-sectional profile of P3EHT$_{100}$-*b*-PT$_{100}$. TEM images of nanostructures from (e) P3EHT$_{100}$-*b*-PT$_{67}$, and (f) P3EHT$_{100}$-*b*-PT$_{100}$. Cryo-TEM images of nanostructures from (g) P3EHT$_{100}$-*b*-PT$_{67}$ and (h) P3EHT$_{100}$-*b*-PT$_{100}$.

larger D_h of 195 nm than that of the nanorods might suggest the structural evolution of the star species from the smaller nanospheres and nanorods (Figure 2). In the case of P3EHT$_{100}$-*b*-PT$_{100}$, a much larger nanostructure resembling a network (nanonetwork) was observed in the AFM images (Figures 3c and S6c). Moreover, the observation that the nanonetwork has the largest D_h (673 nm; determined from DLS) also supported the aforementioned structural evolution (Figure 2). The height of the nanonetwork from P3EHT$_{100}$-*b*-PT$_{100}$ measured by AFM was 5−8 nm. Based on the increase in the height with the increase in the DP of PT, we could confirm the core expansion of the nanostructures. The TEM imaging of the nanostructures confirmed the formation of the nanostar and nanonetwork structures, observed via AFM analysis (Figure 3). Furthermore, one could obtain more details about the nanostructures by TEM, because even without staining, the highly packed crystalline PT core was visible so that even the branching points were visible as well. A closer look at the TEM images of the nanostar and nanonetwork structures revealed that there was minimal contact between the PT cores, as we previously observed for the formation of nanocaterpillar assemblies from PN-*b*-PA via INCP (Figures 3e,f and S6b,c).[9a] In support for this observation, the three-dimensionless side-view and cross-sectional analysis of the high-resolution AFM images revealed that the nanonetwork surfaces were not composed of smooth cylinders; instead, they were highly undulated (Figure 3d), implying that the interconnection of the nanospheres was responsible for the formation of these new nanostructures. Most importantly, the formation of the nanostar and nanonetwork structures in the chloroform solution was further confirmed by cryogenic TEM (cryo-TEM) showing excellent agreement with the images obtained from AFM and TEM in the dry state (Figures 3g,h and S6d,e). This eliminated the possibility that the new nanostructures might have incidentally formed by stacking or overlapping of the nanorods as a result of secondary aggregation during the spin-coating or drop-casting process. Lastly, selected area electron diffraction (SAED) data acquired during the TEM analysis also confirmed the crystallinity of the nanonetwork, showing a distinct diffraction pattern at 0.45 nm that was consistent with the *d*-spacing obtained from PXRD analysis (Figures S3 and S7).

Based on the preponderance of evidence from various analyses presented above, the following mechanism for the formation of these unique branched nanostructures was proposed (Figure 4). Initially, P3EHT-*b*-PT with a low DP of PT spontaneously self-assembled into nanospheres in solution because of the interaction of the solvophobic PT blocks (Figure 4b). Upon further addition of **2**, the core of the nanospheres expanded and became temporarily exposed to the solvent. However, the solvent could no longer solvate these species as the spheres;

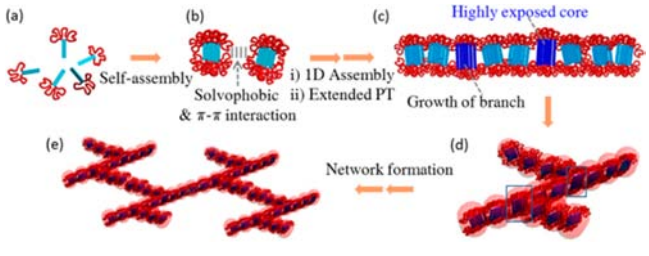

Figure 4. Proposed mechanism for INCP of P3EHT-*b*-PT into branched nanoparticles.

dx.doi.org/10.1021/ja409206p | *J. Am. Chem. Soc.* 2013, 135, 17695−17698

consequently, the core would cling to other nanospheres, thereby forming the nanorods, driven by strong interactions between the exposed PT blocks, to minimize the area of the solvophobic segment (Figure 4c). As more **2** continued to be delivered to the core, a certain portion of the cores in the nanorods further expanded, and nanospheres or nanorods became attached to these highly exposed cores, thereby making these sites the branching points for producing nanostar structures (Figure 4d). Finally, further repetition of this process resulted in the formation of the largest nanostructure—the nanonetwork—which contained the most crystalline PT core (Figure 4e).

The stability of the nanostructures from P3EHT-*b*-PT toward external stimuli such as heat and mechanical stress was evaluated by heating the P3EHT-*b*-PT samples in solution to 80 °C or sonication for 10−30 min because nanofibers consisting of P3HT were normally damaged by sonication.[6a,c] In either case, no significant changes in the UV−vis spectra (maintaining the vibronic features), DLS spectra (maintaining the D_h profiles), and AFM images (maintaining the morphology) were observed (Figures S2, S5, and S9). Thermal gravimetric analysis showed that the block copolymers did not decompose up to 385 °C (Figure S4a). To test the stability of the nanocrystals under even harsher condition, the each of $P3EHT_{100}$-*b*-PT_{33} and $P3EHT_{100}$-*b*-PT_{67} was subjected to continuous heating and washing by Soxhlet extraction with methanol and hexane for ∼40 h. Nevertheless, the integrity of the nanostructures was preserved, as confirmed by AFM and TEM imaging, further supporting the excellent stability of these nanocrystals (Figure S8). The formation of these nanostructures via INCP of the polythiophenes was virtually irreversible because of the large binding force from the tightly packed crystalline cores and the interactions between the cores, holding the nanostructures intact. Lastly, HOMO levels of 5.3 eV were determined for the diblock copolymers via cyclic voltammetry. These deep HOMO levels may be related to the stability of the nanostructures derived from P3EHT-*b*-PT in air, expanding the utility of these nanocrystals much wider (Figure S10).

In conclusion, fully conjugated P3EHT-*b*-PTs were successfully synthesized via the GRIM method, which spontaneously formed highly stable nanoparticles via INCP. The size of the nanocrystals gradually increased with increasing the DP of the PT core, and the evolution of the nanostructures from the nanospheres to nanorods, nanostars, and to nanonetworks was observed. These stable nanocrystals are expected to find useful applications in nano-electronics. Currently, we are also working on other examples of INCP from many polymer derivatives prepared by the GRIM method.

■ ASSOCIATED CONTENT

Supporting Information

Experimental details and further characterization. This material is available free of charge via the Internet at http://pubs.acs.org.

■ AUTHOR INFORMATION

Corresponding Author

tlc@snu.ac.kr

Notes

The authors declare no competing financial interest.

■ ACKNOWLEDGMENTS

Authors dedicate this paper to Prof. Myunghyun Paik Suh on her retirement and 65th birthday. We are grateful for financial support from Basic Science Research, Nano-Material Technology Development, and BRL through NRF of Korea. I.-H.L. is supported by NRF Fostering Core Leaders of the Future Basic Science Program. E.L. is supported by NRF (MSIP, 2011-0014459).

■ REFERENCES

(1) (a) Qian, J.; Zhang, M.; Manners, I.; Winnik, M. A. *Trends Biotechnol.* **2010**, *28*, 84. (b) Li, Z.; Ma, J.; Lee, N. S.; Wooley, K. L. *J. Am. Chem. Soc.* **2011**, *133*, 1228.

(2) (a) Li, Z. B.; Kesselman, E.; Talmon, Y.; Hillmyer, M. A.; Lodge, T. P. *Science* **2004**, *306*, 98. (b) Cui, H.; Chen, Z.; Zhong, S.; Wooley, K. L.; Pochan, D. J. *Science* **2007**, *317*, 647. (c) Dupont, J.; Liu, G. *Soft Matter* **2010**, *6*, 3654. (d) Gröschel, A. H.; Schacher, F. H.; Schmalz, H.; Borisov, O. V.; Zhulina, E. B.; Walther, A.; Müller, A. H. E. *Nat. Commun.* **2012**, *3*, 710.

(3) (a) Rodríguez-Hernández, J.; Chécot, F.; Gnanou, Y.; Lecommandoux, S. *Prog. Polym. Sci.* **2005**, *30*, 691. (b) Kim, J.; Song, I. Y.; Park, T. *Chem. Commun.* **2011**, *47*, 4697. (c) Jang, J.; Kim, J.-K.; Choi, J.-W.; Hwang, T.-S.; Jo, M.; Kim, I.; Cho, B.-K.; Lee, E. *Chem. Commun.* **2013**, *49*, 8003.

(4) (a) Tuncel, D.; Demir, H. V. *Nanoscale* **2010**, *2*, 484. (b) Pecher, J.; Mecking, S. *Chem. Rev.* **2010**, *110*, 6260. (c) Kim, F. S.; Ren, G.; Jenekhe, S. A. *Chem. Mater.* **2011**, *23*, 682.

(5) Li, Z. C.; Ono, R. J.; Wu, Z. Q.; Bielawski, C. W. *Chem. Commun.* **2011**, *47*, 197.

(6) (a) Patra, S. K.; Ahmed, R.; Whittell, G. R.; Lunn, D. J.; Dunphy, E. L.; Winnik, M. A.; Manners, I. *J. Am. Chem. Soc.* **2011**, *133*, 8842. (b) Gilroy, J. B.; Lunn, D. J.; Patra, S. K.; Whittell, G. R.; Winnik, M. A.; Manners, I. *Macromolecules* **2012**, *45*, 5806. (c) Gwyther, J.; Gilroy, J. B.; Rupar, P. A.; Lunn, D. J.; Kynaston, E.; Patra, S. K.; Whittell, G. R.; Winnik, M. A.; Manners, I. *Chem.—Eur. J.* **2013**, *19*, 9186. (d) Kamps, A. C.; Fryd, M.; Park, S.-J. *ACS Nano* **2012**, *6*, 2844.

(7) (a) Wu, P.-T.; Ren, G.; Li, C.; Mezzenga, R.; Jenekhe, S. A. *Macromolecules* **2009**, *42*, 2317. (b) He, M.; Zhao, L.; Wang, J.; Han, W.; Yang, Y.; Qiu, F.; Lin, Z. *ACS Nano* **2010**, *4*, 3241. (c) Hammer, B. A. G.; Bokel, F. A.; Hayward, R. C.; Emrick, T. *Chem. Mater.* **2011**, *23*, 4250.

(8) Lee, E.; Hammer, B.; Kim, J.-K.; Page, Z.; Emrick, T.; Hayward, R. C. *J. Am. Chem. Soc.* **2011**, *133*, 10390.

(9) (a) Yoon, K.-Y.; Lee, I.-H.; Kim, K. O.; Jang, J.; Lee, E.; Choi, T.-L. *J. Am. Chem. Soc.* **2012**, *134*, 14291. (b) Kim, J.; Kang, E.-H.; Choi, T.-L. *ACS Macro Letters* **2012**, *1*, 1090.

(10) (a) Scherf, U.; Gutacker, A.; Koenen, N. *Acc. Chem. Res.* **2008**, *41*, 1086. (b) Xin, H.; Kim, F. S.; Jenekhe, S. A. *J. Am. Chem. Soc.* **2008**, *130*, 5424. (c) Xin, H.; Ren, G.; Kim, F. S.; Jenekhe, S. A. *Chem. Mater.* **2008**, *20*, 6199. (d) Li, L.; Lu, G.; Yang, X. *J. Mater. Chem.* **2008**, *18*, 1984. (e) Kim, J. S.; Lee, J, H.; Park, J. H.; Shim, C.; Sim, M.; Cho, K. *Adv. Funct. Mater.* **2011**, *21*, 480.

(11) (a) Jung, Y.; Ko, D. K.; Agarwal, R. *Nano Lett.* **2007**, *7*, 264. (b) Li, Z.; Li, W.; Camargo, P. H. C.; Xia, Y. *Angew. Chem., Int. Ed.* **2008**, *47*, 9653. (c) Miszta, K.; de Graaf, J.; Bertoni, G.; Dorfs, D.; Brescia, R.; Marras, S.; Ceseracciu, L.; Cingolani, R.; van Roij, R.; Dijkstra, M.; Manna, L. *Nat. Mater.* **2011**, *10*, 872.

(12) (a) Yan, H.; Yan, Y.; Yu, Z.; Wei, Z. *J. Phys. Chem. C* **2011**, *115*, 3257. (b) Mohd Yusoff, S. F.; Gilroy, J. B.; Cambridge, G.; Winnik, M. A.; Manners, I. *J. Am. Chem. Soc.* **2011**, *133*, 11220. (c) Qiu, H.; Cambridge, G.; Winnik, M. A.; Manners, I. *J. Am. Chem. Soc.* **2013**, *135*, 12180.

(13) Loewe, R. S.; Ewbank, P. C.; Liu, J.; Zhai, L.; McCullough, R. D. *Macromolecules* **2001**, *34*, 4324.

(14) Ihn, K. J.; Moulton, J.; Smith, P. *J. Polym. Sci., Part B: Polym. Phys.* **1993**, *31*, 735.

(15) Mo, Z.; Lee, K.-B.; Moon, Y. B.; Kobayashi, M.; Heeger, A. J.; Wudl, F. *Macromolecules* **1985**, *18*, 1972.

(16) Ho, V.; Boudouris, B. W.; Segalman, R. A. *Macromolecules* **2010**, *43*, 7895.